Clumped isotope evidence for Early Jurassic extreme polar warmth and high climate sensitivity

Thomas Letulle[1], Guillaume Suan[1], Mathieu Daëron[2], Mikhail Rogov[3], Christophe Lécuyer[1], Arnauld Vinçon-Laugier[1], Bruno Reynard[1], Gilles Montagnac[1], Oleg Lutikov[3], Jan Schlögl[4].

5   [1] Univ Lyon, UCBL, ENSL, UJM, CNRS, LGL-TPE, F-69622, Villeurbanne, France

[2] Laboratoire des Sciences du Climat et de l'Environnement, LSCE/IPSL, CEA-CNRS-UVSQ, Université Paris-Saclay, Orme des Merisiers, F-91191 Gif-sur-Yvette Cedex, France

[3] Geological Institute of Russian Academy of Sciences, Laboratory of Phanerozoic Stratigraphy.

[4] Comenius University, Faculty of Natural Sciences, Department of Geology and Palaeontology, Mlynská dolina

10   G, 842 15 Bratislava, Slovak Republik

Correspondence to: Thomas Letulle (thomas.letulle@univ-lyon1.fr)

Abstract. Periods of high atmospheric CO_2 levels during the Cretaceous-Early Paleogene (~140 to 33 My ago)

15   were marked by very high polar temperatures and reduced latitudinal gradients relative to the Holocene. These features represent a challenge for most climate models, implying either higher-than-predicted climate sensitivity to atmospheric CO_2, or systematic biases or misinterpretations in proxy data. Here, we present a reconstruction of marine temperatures at polar (>80°) and mid (~40°) paleolatitudes during the Early Jurassic (~180 My ago) based on the clumped isotope (Δ_{47}) and oxygen-isotope ($\delta^{18}O_c$) analyses of mildly buried pristine mollusc shells.

20   Reconstructed calcification temperatures range from ~8 to ~18°C in the Toarcian Arctic and from ~24 to ~28 °C in Pliensbachian mid-paleolatitudes. These polar temperatures were ~10-20°C higher than present along with reduced latitudinal gradients. Reconstructed seawater oxygen isotope values ($\delta^{18}O_w$) of – 1.5 to 0.5‰ VSMOW and of – 5 to – 2.5‰ VSMOW at mid and polar paleolatitudes, respectively, point to a significant freshwater contribution in Arctic regions. This highlight the risk of assuming the same $\delta^{18}O_{sw}$ value for $\delta^{18}O$-derived

25   temperature from different oceanic regions. These findings provide critical new constraints for model simulations of Jurassic temperatures and $\delta^{18}O_{sw}$ values and suggest that high climate sensitivity is a hallmark of greenhouse climates since at least 180 My.

1 Introduction

30   Proxy data indicate that the Cretaceous-Early Paleogene (~140 to 33 My ago) was characterized by high atmospheric CO_2 concentrations, extreme polar warmth and reduced latitudinal temperature gradients (Sluijs et al., 2006; Suan et al., 2017; Evans et al., 2018). Most state-of-the-art climate models hardly reproduce such features, implying either a higher climate sensitivity under greenhouse conditions or systematic biases in proxy data interpretation (Huber and Caballero, 2011; Zhu et al., 2020; Laugié et al., 2020). It remains unclear whether

35   higher climate sensitivity is unique to the Cretaceous-Early Paleogene world or is rather a hallmark of Earth's climate under high atmospheric pCO_2. Temperature proxies sensitive to burial, such as molecular or clumped-isotope thermometry, have seldom been applied to older sediments owing to their generally higher thermal maturity (Robinson et al., 2017; Ruebsam et al., 2020; Fernandez et al., 2021). Consequently, current

temperature estimates for ante-Cretaceous periods are mostly derived from the oxygen isotope composition of
marine carbonate fossils ($\delta^{18}O_c$), with well-known limitation related to uncertainties in the past $\delta^{18}O$ signature of
seawater ($\delta^{18}O_w$) (Epstein et al., 1953; Roche et al., 2006; Laugié et al., 2020).

Here, we use carbonate clumped isotope thermometry (Δ_{47}), to simultaneously constrain the calcification
temperatures and associated $\delta^{18}O_w$ values of marine carbonate shells collected from Lower Jurassic sedimentary
successions with exceptionally shallow to moderate burial depths spanning subtropical to polar paleolatitudes.

We compare our results to existing Jurassic to Eocene climate proxy data and simulations and discuss their
implications for climate sensitivity under greenhouse conditions.

2 Geological settings

2.1 Polovinnaya River

The Polovinnaya River section is located in northern Siberia (72°36'05" N, 107°58'52.2" E), and was located
near the north pole during the early Jurassic (Fig. 1). Our bivalve samples come from between 0 and 14m in the
section and belong to the Toarcian (Suan et al., 2011). This interval consists of silty shale slightly enriched in
organic carbon (TOC ~0.5%). Except for localized carbonate concretions, there is no carbonate fraction in the
sediment. The studied interval has been previously correlated to the lower Toarcian Serpentinum ammonite zone
based on biostratigraphy of foraminifera and dinoflagellate cyst, and lithostratigraphic correlation with other
sections of the basin (Suan et al., 2011). This section records very abundant *Dacryomya* bivalve shells (Fig. S1),
an opportunistic suspension-feeder genus tolerant to poorly oxygenated waters, which preferred conditions with
weak hydrodynamics (Zakharov and Shurygin, 1978). Few belemnite rostra were also recorded as well isolated
fish scales and teeth. The section undergone exceptionally low burial as suggested by the low values of Rock-
Eval Pyrolysis T_{max} (mean = 420°C) previously measured in the host sediments (Suan et al., 2011). Regional
stratigraphy from the more distal Anabar area suggest local overburden not exceeding 1000m: a total overburden
(Lower Toarcian to Valanginian) of about 380m is recorded in the Anabar River area (Nikitenko et al., 2013)
located 200 km East of the Polovinnaya section, which may be extended to about 1000m when adding
Valanginian-Cenomanian overburden from the more distal Bol'shoi Begichev islands. Modern local geothermal
fluxes are lower than 50 mWm^{-2} (Kerimov et al., 2020), indicative of low geothermal gradient (<25°C/km).
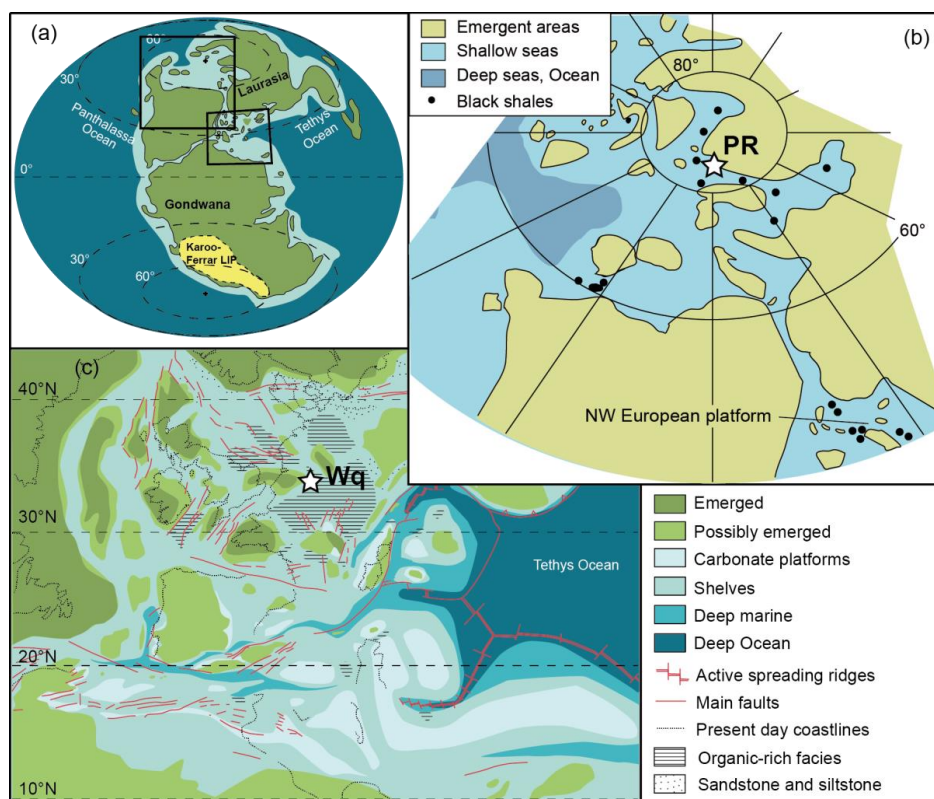
Figure 1. Location of the studied sites with regard to Toarcian (Early Jurassic) geography. (a) Global map
modified from Dera et al. (2009). (b) Arctic map modified from Nikitenko and Mickey (2004). (c) Tethyan map
modified from Thierry, (2000). Localities: PR = Polovinnaya River; Wq = Warcq.

2.2 Warcq

Samples from north-eastern Paris Basin were collected in 2014 from a temporary road cutting located near
Warcq, Ardennes, France (49°45'21.6"N 4°39'28.8"E). They consist of grey silty claystone with lenses of packed
carbonated shell fragments, mainly from a variety of bivalves (*Grammatodon, Malletia, Limea, Oxytoma*) and
few ammonoids (*Beaniceras, Aegoceras?,* Dactyloceratidae) (Fig. 2). The lithology, fossil preservation and
assemblages of the sampled beds is similar to those described by Thuy et al. (2011), from a nearby site of Sedan
and dated from the Pliensbachian Davoei zone. The sampled levels are therefore tentatively attributed to the
lower Pliensbachian Davoei ammonite zone. Mean T_{max} values of 425°C and maximum burial temperatures near
60°C have been reported for Pliensbachian sediments of the NE Paris Basin (Disnar et al., 1996; Blaise et al.,
2014). These burial temperatures should be regarded as an upper limit, as the very proximal sampling area near
Warcq was repeatedly emerged during the Mesozoic and hence shows a much-thinner Mesozoic cover than these
more distal sites (Waterlot et al., 1960).
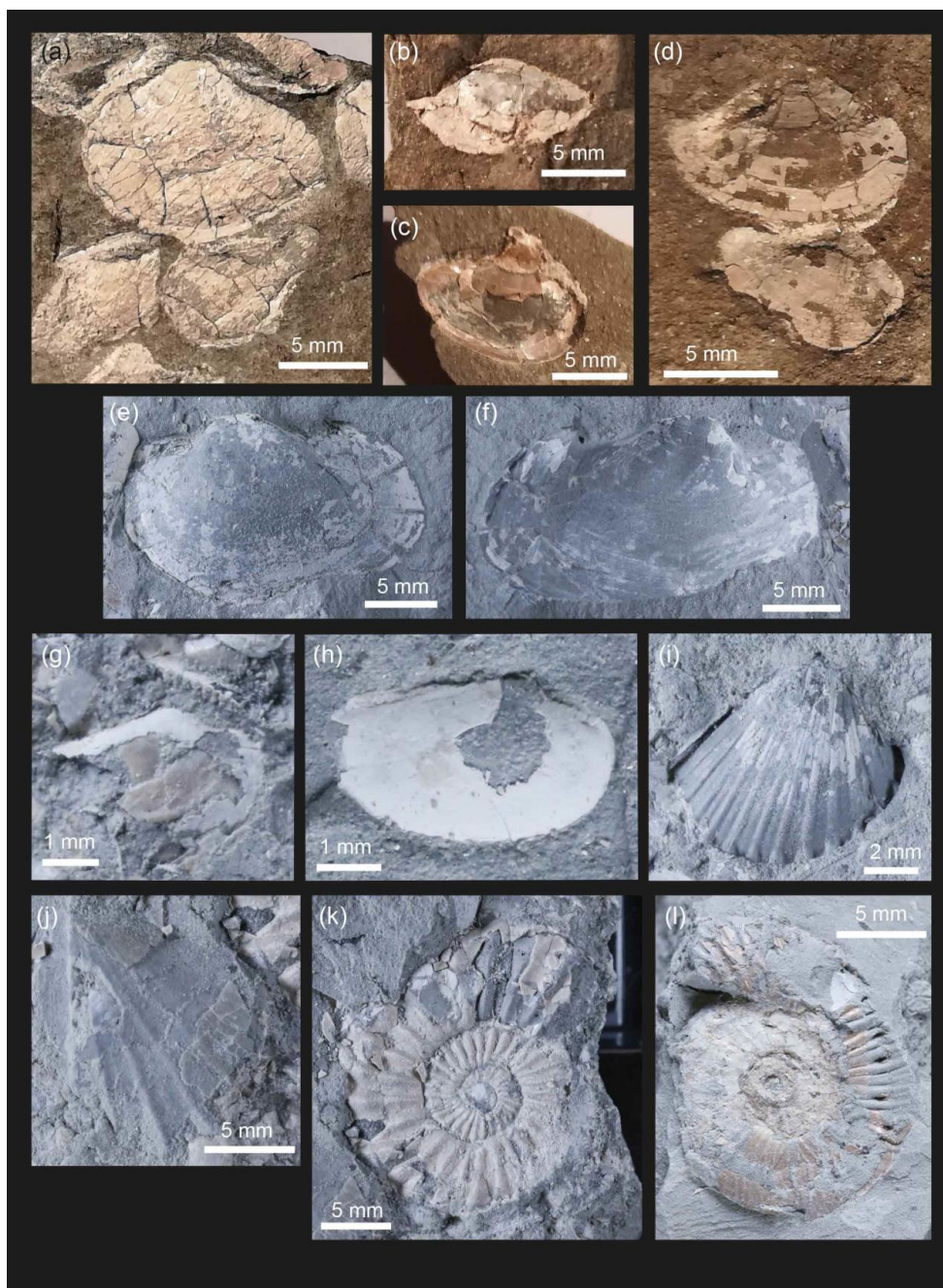
Figure 2. Selected specimens from the sampled successions. (a-d). Polovinnaya River section (Toarcian), (e-l). Warcq section (Pliensbachian); (a). *Dacryomya jacutica*, specimen Pol 29; (b). *Dacryomya jacutica*, specimen Pol 13; (c-d). *Dacryomya jacutica*, specimen Pol 5; (e-f). *Grammatodon* sp., specimen ARD-01; (g-h). *Malletia*

90

sp.; (i). *Limea* sp., specimen ARD-03; (j). *Oxytoma* sp.ind. (k). *Aegoceras?*, specimen ARD 06; (l).
Dactylioceratidae indet., specimen ARD-07.

3 Material and Methods

95

3.1 Sampled material

The two studied sites present exceptionally rare records of aragonite preservation for the Lower Jurassic interval.
Dacryomya shells are the most abundant macrofossil and the unique bivalve genera to occur in the Polovinnaya
River section. They are very abundant in the lower part of the section (0 to 8m). They are mainly represented by

100   adult shells, while juveniles are common in only few levels. They appear as ~1cm distinct individual or detached
valves, sometimes close to each other (Fig. 2). The carbonate shells, often flattened and partially to entirely
preserved, are a few millimetres thick but brittle and detached easily from their inner and outer mould. Their
cream to white colour contrasts with the dark aspect of the sediment, and few thicker individuals are iridescent.
Molluscs shells from Warcq, clearly show a more energetic environment as they mostly appear as packed shell

105   fragments showing a higher taxonomic diversity relative to the other site. Few complete individuals and
separated valves can be observed among the debris with their associated mould in or around the remaining shell.
Shells are cream to clear white, with some showing iridescence.

The microstructural preservation state and mineralogy of the analysed bivalve and ammonite shells were
investigated using a Phenom Pure G2 scanning electron microscope in backscatter mode (BSEM G2) and Raman

110   spectroscopy using an XploRA Raman microscope in Laboratoire de Géologie de Lyon (LGLTPE).

3.2 Geochemical analysis and data processing

The remnants of carbonate shells were sampled as a whole using dental tools under a binocular-microscope. A

115   carbonate vein and matrix from the carbonate nodule Pol 29 were also sampled to constrain the geochemistry of
this potential diagenetic phase.

The Δ_{47} and $\delta^{18}O$ values of 13 samples were measured (1 to 5 replicates each) using methods described by
(Daëron et al., 2016). Carbonate samples were converted to CO_2 by phosphoric acid reaction at 90 °C in a
common, stirred acid bath for 15 minutes. Initial phosphoric acid concentration was 103 % (1.91 g/cm3) and

120   each batch of acid was used for 7 days. After cryogenic removal of water, the evolved CO2 was helium-flushed
at 25 mL/mn through a purification column packed with Porapak Q (50/80 mesh, 1 m length, 2.1 mm ID) and
held at −20 °C, then quantitatively recollected by cryogenic trapping and transferred into an Isoprime 100 dual-
inlet mass spectrometer equipped with six Faraday collectors (m/z 44–49). Each analysis took about 2.5 hours,
during which analyte gas and working reference gas were allowed to flow from matching, 10 mL reservoirs into

125   the source through deactivated fused silica capillaries (65 cm length, 110 μm ID). Every 20 minutes, gas
pressures were adjusted to achieve m/z = 44 current of 80 nA, with differences between analyte gas and working
gas generally below 0.1 nA. Pressure-dependent background current corrections were measured 12 times for
each analysis. All background measurements from a given session are then used to determine a mass-specific
relationship linking background intensity (Zm), total m/z = 44 intensity ($I44$), and time (t): $Zm = a + bI44 + ct +$

130    $dt2$. Background-corrected ion current ratios ($\delta45$ to $\delta49$) were converted to $\delta13C$, $\delta18O$, and "raw" $\Delta47$ values

as described by Daëron et al., (2016), using the IUPAC oxygen-17 correction parameters. The isotopic composition ($\delta 13C$, $\delta 18O$) of our working reference gas was computed based on the nominal isotopic composition of carbonate standard ETH-3 (Bernasconi et al., 2018) and an oxygen-18 acid fractionation factor of 1.00813 (Kim et al., 2007). Raw $\Delta 47$ values were then converted to the I-CDES $\Delta 47$ reference frame by

135   comparison with four "ETH" carbonate standards (Bernasconi et al., 2021) using a pooled regression approach (Daëron, 2021). Full analytical errors are derived from the external reproducibility of unknowns and standards (Nf = 89) and conservatively account for the uncertainties in raw $\Delta 47$ measurements as well as those associated with the conversion to the "absolute" $\Delta 47$ reference frame.

Complementary $\delta^{13}C$ and $\delta^{18}O$ analyses of the smallest Arctic shells were performed at LGLTPE, using a

140   Multiprep^{TM} automated sampler coupled to a dual-inlet GV Isoprime^{TM} mass spectrometer. Samples were reacted with anhydrous phosphoric acid at 90°C. Duplicated samples were adjusted to the international references NIST NBS 18 and NBS 19 as well as in-house standard Carrara Marble. Since 2019 overall reproducibility of the in-house standard Carrara Marble are ±0.082 for $\delta^{18}O$ (2 SE, n = 441) and ±0.057 ‰ for $\delta 13C$ (2 SE, n = 441) with mean $\delta^{18}O$ and $\delta^{13}C$ values respectively of - 1.041 ‰ and +2.025 ‰ (V-PDB). All

145   carbonate isotopic values ($\delta^{13}C$, $\delta^{18}O_c$) are reported in ‰ VPDB.

Clumped isotope temperatures were computed based on the I-CDES calibration of (Anderson et al., 2021). Temperature uncertainties correspond to the fully-propagated 95% confidence intervals from Δ_{47} measurements of each sample (Daëron, 2021), neglecting the much smaller uncertainties in the calibration. The $\delta^{18}O$ values from aragonite samples were adjusted considering the different phosphoric acid fractionation factors for calcite

150   and aragonite (Kim et al., 2007). The $\delta^{18}O_w$ values relative to VSMOW was estimated using Δ_{47}-derived temperatures and the equations of Grossman and Ku (1986) and Kim and O'Neil (1997) for mollusc shells and calcite vein respectively.

Paleolatitude of the studied sites was computed using the online paleolatitude calculator paleolatitude.org (van Hinsbergen et al., 2015) computed with the model of Torsvik et al. (2012).

155

4 Results

The SEM observations of shell fragments of *Dacryomya jacutica* revealed well preserved sheet nacreous microstructures underlying a prismatic layer we interpret as the outer shell layer (Fig. 3). All Raman spectra gathered from *Dacryomya jacutica* shells confirm that the original aragonite mineralogy is preserved. Mollusk

160   shells from Warcq showing an aragonite mineralogy revealed microstructures similar to those observed in *Dacryomya jacutica*, the main differences being that sheet nacreous structures of the studied ammonite shell (ARD-05) shows thinner tablets than those of bivalve shells (Fig. 3). Both SEM and Raman data indicate that the sample ARD-03 (bivalve fragment) is in calcite, showing a darker colour and no iridescence, with a much simpler and massive structure observed in SEM (Fig. 3).

165   Reconstructed Δ_{47} temperatures range from 8.5±5.2°C to 17.7±3.4°C for Siberian bivalves, from 24.1±4.38°C to 27.6±3.3 °C for molluscs from NE France, while for the fracture-infilling calcite vein from Siberia a temperature of 31.1 ± 4.8 °C is inferred. Mean $\delta^{18}O_c$ values are -2.73 ±0.71‰ (1SD, n=31, Max=0.36, Min=-5.08‰) for Siberian bivalves and -14.21 ± 0.02 ‰ for the fracture-infilling calcite vein, and -2.07 ± 0.86‰ (1SD, n=4, Max=-0.84‰, Min=-2.54‰) for molluscs from NE France. The carbon isotope values ($\delta^{13}C$) range from 0.37‰

170   to 2.82‰ in the selected molluscs from Warcq, from 3.47‰ to 5.09‰ in the Russian Arctic bivalves, and reach

values down to -21.43‰ and -4.67‰ for carbonate nodule matrix and the embedded bivalve shells (sample POL-29) respectively.

The calculated $\delta^{18}O_w$ values range from 0.5±0.7‰ to -1.5±1.0‰ in molluscs from NE France, from -4.88±1.20‰ to -2.52±0.78‰ in Siberian bivalves. A much lower value of -10.6 ±0.9‰ is obtained for the

175   fracture-infilling calcite vein from Polovinnaya River.
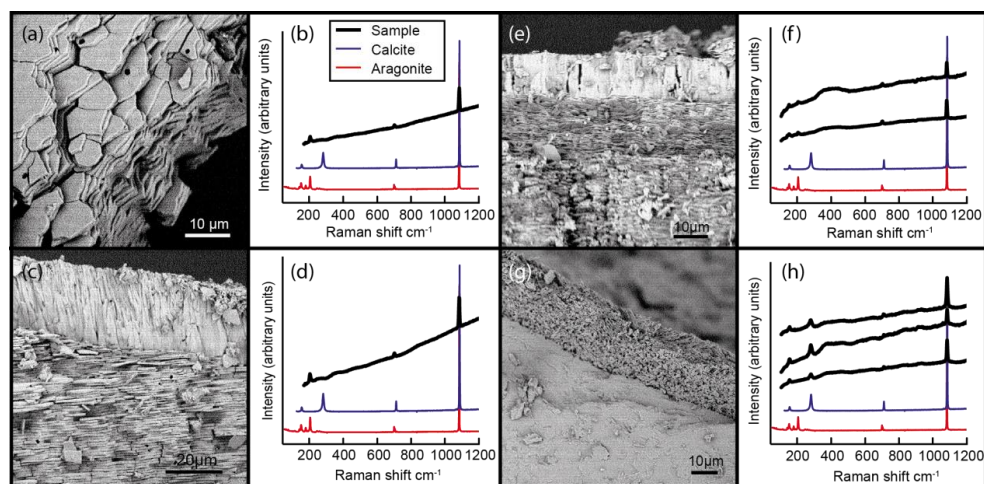
Figure 3. SEM images and Raman spectra for a selection of samples. a, c, e and g SEM images form samples POL-8, POL-12, ARD-05 and ARD-03 respectively. b, d, f and g Raman spectra from samples POL-8, POL-12,

180   ARD-05 and ARD-03 compared to the reference spectra of calcite and aragonite.

5 Discussion

5.1 Sample preservation

185   The SEM and Raman observations reveal that the analysed mollusc shells from both sites retain pristine aragonite mineralogy and microstructures with no evidence of recrystallization (Fig. 3). Despite their aragonite mineralogy, the *Dacryomya* shells from sample Pol-29 record unusually low $\delta^{13}C$ that are ~8‰ lower than the other *Dacryomya* shells analysed from the same succession. The carbonate matrix of the nodule where these shells are embedded also records a very low $\delta^{13}C$ value (-21.43‰) but a $\delta^{18}O$ value within the range of the

190   bivalve shells. We therefore attribute the extremely low $\delta^{13}C$ values of bivalves shells of this level to an early diagenetic phase resulting in the formation of carbonate nodules derived from respiratory CO_2 that locally altered the bivalve shells geochemistry.

Organic matter maturity, mineralogical and sedimentological data all imply exceptionally shallow burial depth (<1 km) for the samples investigated here. Maximum burial temperature (T_{burial}) remained well below the

195   commonly assumed minimum temperature (80-120°C) of solid-state reordering of C-O bonds at geological timescales (Henkes et al., 2014; Stolper and Eiler, 2015; Hemingway and Henkes, 2021). The exceptional preservation of aragonite nacreous sheet microstructures in these samples imply minimal amounts of fluid circulation and recrystallization, if any. Exchange between fluid inclusions in mollusc shells and the surrounding

carbonate minerals was recently suggested as an alternative process that may alter the clumped isotope signature

200 of biogenic carbonates without substantially affecting the stable isotope signature of the shell nor its mineralogy (Nooitgedacht et al., 2021). In their heating experiments, these exchanges resulted in a significant decrease of the Δ_{47} value of the bivalve shells compared to the original shell, and a minor (~0.1‰) decrease in $\delta^{18}O$ of the heated shell. We cannot exclude that this process has altered the fossils studied here even at low temperature, nor do we have evidence that it occurred. The Δ_{47} temperature of 31.1 ± 4.8 °C for the fracture-infilling calcite vein

205 in Arctic Russia is significantly higher than those inferred from bivalves and is consistent with a formation depth <1 km assuming a geothermal gradient of 25°C/km. The reconstructed $\delta^{18}O_w$ value of –10.7± 0.9 ‰ for this calcite vein is also substantially lower than those inferred from associated bivalves, consistent with a late-phase meteoric source for the mineralizing fluid.

210 **5.2 Evidence for extreme warmth and reduced salinity in the Arctic during the Toarcian Oceanic Anoxic Event**

Bivalve shells record a marked rise in $\delta^{13}C$ along the section up to ~5‰ that parallels that recorded by organic carbon $\delta^{13}C$ data (Fig. 4; Suan et al., 2011). These results strengthen the correlation of the corresponding part of the succession with the rising limb of the positive carbon isotope excursion commonly used to characterise the

215 termination of T-OAE interval in coeval sites of Europe and North Africa (Jenkyns and Clayton, 1986; Suan et al., 2010; Krencker et al., 2014; Ullmann et al., 2020; Baghli et al., 2020). Bivalve shells $\delta^{18}O_c$, however, show no stratigraphic trend as opposed to brachiopod shell T-OAE records from mid-latitudes (Suan et al., 2010; Krencker et al., 2014; Ullmann et al., 2020; Baghli et al., 2020). Our Δ_{47} results yield polar temperatures ranging from 8.5±5.2 to 17.7±3.4 °C. As it occurs with most Δ_{47}-derived temperature datasets, the relatively large

220 uncertainties of the present estimates of Siberian SST hamper the identification of distinctive stratigraphic trends.

Bivalve shell growth can be highly variable during the animal life (Schöne, 2008), making any paleoenvironmental record derived from bivalve shell either incomplete (because of growth cessation) or at least biased towards the period of maximum growth rate. Shell growth rate can be controlled by both environmental

225 parameters (Temperature, salinity, food availability …), biological processes such as spawning and ontogeny (Schöne, 2008). One major aspect of shell growth that may bias the geochemical signal data is seasonal shell growth-cessation. In modern high latitude bivalves, seasonal shell growth-cessation generally occurs during the winter, triggered by low temperatures or low food availability (Peck et al., 2000; Vihtakari et al., 2016; Killam and Clapham, 2018).

230 It appears likely that food availability declined markedly during the Early Jurassic polar night, which would have certainly led to winter growth cessation in the analysed *Dacryomya* shells. In the present-day *Nucula annulata*, an aragonite bivalve with similar ecology to the analysed *Dacryomya jacutica*, growth cessation occurs in winter and during spawning at peak local temperatures, its average $\delta^{18}O_c$ hence records late spring to early fall SST (Craig, 1994). By contrast, growth band $\delta^{18}O_c$ offers evidence for summertime-only growth cessation in high-

235 latitude Eocene bivalves from Antarctica, with inferred winter SST of 11.1±0.6 and summer SST of 17.6±1.3°C (Buick and Ivany, 2004; Douglas et al., 2014) very close to our maximal and minimum SST estimates of the Toarcian Arctic. A comparable seasonal $\delta^{18}O_c$ record could not be generated from our Russian Arctic material owing to the very small size of the available *Dacryomya* shells (1 to 2cm). In any case, the temperate data from

NE France should be minimally affected by seasonal biases as shell precipitation occurs more continuously
240   throughout the year in modern temperate molluscs (Killam and Clapham, 2018). Besides, both sites were
deposited in near shore environments at very shallow depths likely not exceeding a few tens of meters (Thuy et
al., 2011; Suan et al., 2011). Although bivalves from both sections record temperatures near the sea bottom that
were likely slightly cooler than the sea surface, the difference should not exceed a few degrees. We therefore
conservatively interpret the reconstructed temperatures as reflecting polar warm-season SST (summer; SST_{PWS})
245   in Arctic Russia and low latitude annual SST in NE France. These SST_{PWS} for the T-OAE are still 10-20°C
higher than present-day SST_{PWS} (Fig. 5).

The reconstructed polar $\delta^{18}O_w$ values ranging from – 4.9 ±1.2 to –2.5 ±0.8‰ during the T-OAE are significantly
lower than the value of –1‰ expected for an ice-free world mean open ocean (Shackleton and Kennett, 1975).
These results imply a substantial freshwater contribution to the studied basin during the T-OAE, probably
250   resulting from coastal runoff at this relatively proximal site, as evidenced from abundant terrestrial organic
matter (Suan et al., 2011). High temperatures and reduced salinity are in broad agreement with paleontological
evidence for warm and humid temperate conditions during the T-OAE interval in Arctic Siberia (Rogov et al.,
2019). Arctic coast salinity can be inferred from Δ_{47}-derived $\delta^{18}O_w$ with reasonable assumptions of local $\delta^{18}O$ of
precipitations and runoff ($\delta^{18}O_p$). Higher polar temperatures should have produced higher $\delta^{18}O_p$ than those
255   prevailing today (Rozanski et al., 1992), a hypothesis supported by terrestrial plants *n*-alkanes hydrogen isotopes
and paleosol siderite Δ_{47} data indicating Early Eocene $\delta^{18}O_p$ of –10 to –15‰ (Pagani et al., 2006; van Dijk et al.,
2020). Assuming a similar range of $\delta^{18}O_p$ values in the Early Jurassic Arctic, and a global mean ocean with a
salinity of 34.5‰ and a $\delta^{18}O_w$ of –1‰, mass balance calculations indicate mean salinity of 23.9±2.9‰ (1σ, n=8)
and 27.7±1.8‰ (1σ, n=8) with $\delta^{18}O_p$ of –10 and –15‰, respectively (see Supplementary Data). These estimates
260   point towards brackish waters at Polovinnaya River during the Toarcian, consistent with the fossil assemblages
of the succession that includes abundant terrestrial organic matter and wood debris, marine to brackish elements
such as abundant dinoflagellate cysts, benthic foraminifera (preserved as organic linings and agglutinate forms)
but rarer typically marine elements that are only represented by a few belemnite rostra and unidentifiable
ammonite internal moulds (Suan et al., 2011). Such values are also comparable to the salinity of 28‰ estimated
265   using a fully coupled ocean–atmosphere model for the Toarcian (Dera and Donnadieu, 2012), although the
Arctic temperature obtained by the same model are in strong disagreement with our data (Fig. 5). Such
observations should be replicated around the Arctic realm to test whether the brackish environment evidenced
here is of local or more regional nature.
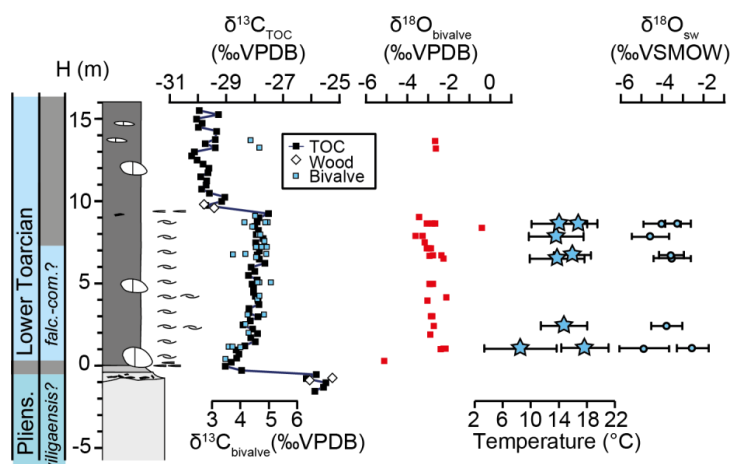
Figure 4. Geochemical record of the T-OAE at Polovinnaya River, Arctic Siberia. Stratigraphy and organic carbon isotope ($\delta^{13}C_{TOC}$) data from Suan et al. (2011). The analysed bivalve samples all belong to the species *Dacryomya jacutica*. Δ_{47}-derived temperatures were computed using the equation of Anderson et al. (2021). $\delta^{18}O_w$ was calculated using the oxygen isotope fractionation equation of Grossman and Ku (1986).

5.3 Early Jurassic latitudinal temperature and $\delta^{18}O_w$ gradients

The mid paleolatitude SST reconstructed by our new clumped isotope data are in good agreement with recent Sinemurian-Pliensbachian and Toarcian TEX$_{86}$^{H} data pointing to summer SST~20-30°C at slightly lower paleolatitudes (Robinson et al., 2017; Ruebsam et al., 2020). Considering the scarcity of other Early Jurassic temperature proxy-data, model-based SST and $\delta^{18}O_w$ estimates, we extend the comparison to SST and $\delta^{18}O_w$ estimates based on various proxy-data and published Earth system simulations for other Jurassic to Eocene intervals (Fig. 5; Supplement). This compilation shows that Δ_{47} SST from NE France agree with most previous TEX$_{86}$^{H} and Δ_{47} SST for the Jurassic-Eocene interval, with values > 5°C higher than present-day SST. This comparison also shows that the Maastrichtian was characterized by substantially lower Δ_{47} SST, in line with independent evidence for global cooling during this interval (O'Brien et al., 2017; Pucéat et al., 2003), although many Δ_{47} records from this stage come from the Western Interior Seaway (WIS) where temperatures were likely influenced by specific regional patterns, such as southward influence of arctic water or significant freshwater contribution in the basin (Coulson et al., 2011; Petersen et al., 2016). This compilation also reveals lower SSTs near 50°N in the Callovo-Oxfordian. Russian Arctic SST are very close to Campanian-Maastrichtian and Early Eocene TEX$_{86}$^{H}-derived SST (Jenkyns et al., 2004; Sluijs et al., 2020) and Early Eocene bioclimatic SST (Suan et al., 2017) from the Arctic (Fig. 5). The Δ_{47} data presented herein suggest a decrease in mean SST of 0.26±0.05°C per ° of latitude, i.e., a reduction of the latitudinal SST gradient of 32±10% relative to present, consistent with the most conservative Early Eocene estimates (Evans et al., 2018).

Our Δ_{47} SST for the Lower-Jurassic can be compared to published results from Earth System models that simulate past intervals of global warmth to discuss model-data discrepancies. Proxy-data indicate an atmospheric pCO$_2$ of 1000±500 ppmv during the Early Jurassic, with maximum values of 1750±500 ppmv, i.e., 6x pre-industrial levels (PIL), during the T-OAE (McElwain et al., 2005; Li et al., 2020). Earth system models run at 6x PIL for Early Jurassic (Dera and Donnadieu, 2012) or Cretaceous-Eocene paleogeography almost invariably

produce lower SST than those inferred from our Δ_{47} data, with a maximum model-data discrepancy of >15°C at high latitudes (Fig. 5). To achieve such polar warmth, the Eocene CCSM3 simulations require 16x PIL, more

300   than twice that indicated by Lower Jurassic and Eocene proxy data (Huber and Caballero, 2011). Reconstructed SST of 14.4 ±2.8°C near the North Pole during the T-OAE, however, correspond to the maximum monthly temperatures simulated by the Turonian IPSL-CM5A2 model near the North Pole at 4x PIL (Laugié et al., 2020). The hypothesis of shell growth restricted to warmest month in the analysed Toarcian Arctic bivalves, however, remains questionable given the evidence for summertime-only growth cessation in Eocene bivalves from

305   Antarctica (Buick and Ivany, 2004). Finally, Arctic SST as high as 15-20°C are successfully achieved in the Eocene CESM1.2 CAM5 at 6 to 9x PIL (Zhu et al., 2020), in which climate sensitivity increases with rising CO_2 due to low-altitude cloud albedo feedbacks and improved radiative parameterization. As this model produces an increase in climate sensitivity with CO_2 in both Eocene and modern conditions, our results thus support the growing body of evidence that the amplitude of the future anthropogenic warming may be underestimated by

310   conventional state-of-the-art models.

The reconstruction of $\delta^{18}O_w$ values using proxy data provides a complementary aspect to assess model capabilities, as this indicator is sensitive to both climate parameters (moisture, humidity and temperatures) and paleogeography. Our mid-latitude $\delta^{18}O_w$ are broadly similar to those reconstructed using marine turtle bones $\delta^{18}O_{PO4}$ and Δ_{47} data from Jurassic to Eocene bivalves, ammonites, foraminifera, as well as belemnites (Fig. 5).

315   As for temperatures, regional processes in the Western Interior Seaway explains the mid latitude very low $\delta^{18}O_w$ indicated by most late Cretaceous Δ_{47} data (Petersen et al., 2016).

We are aware of only few Earth-system $\delta^{18}O_w$ simulations for the interval considered here (Zhou et al., 2008; Tindall et al., 2010; Zhu et al., 2020), hence limiting model-data comparisons. The higher freshwater contribution near high-latitude landmasses of the Northern Hemisphere in both models produced lower $\delta^{18}O_w$

320   that are broadly consistent with previous and our proxy data (Fig. 5). This good agreement, however, might be partly fortuitous, as proxy data suggest SST much higher than those produced by both models (Fig. 5). As mentioned above, such higher-than-predicted polar warmth would have substantially increased high-latitude $\delta^{18}O_p$, so that higher runoff would be required to reproduce the magnitude of the poleward drop in $\delta^{18}O_w$ indicated by proxy data. This highlights the usefulness, in future models of past greenhouse climates, to

325   systematically provide $\delta^{18}O_w$ predictions so that $\delta^{18}O_w$ estimates derived from Δ47 data may serve as a constraint on Earth system models.
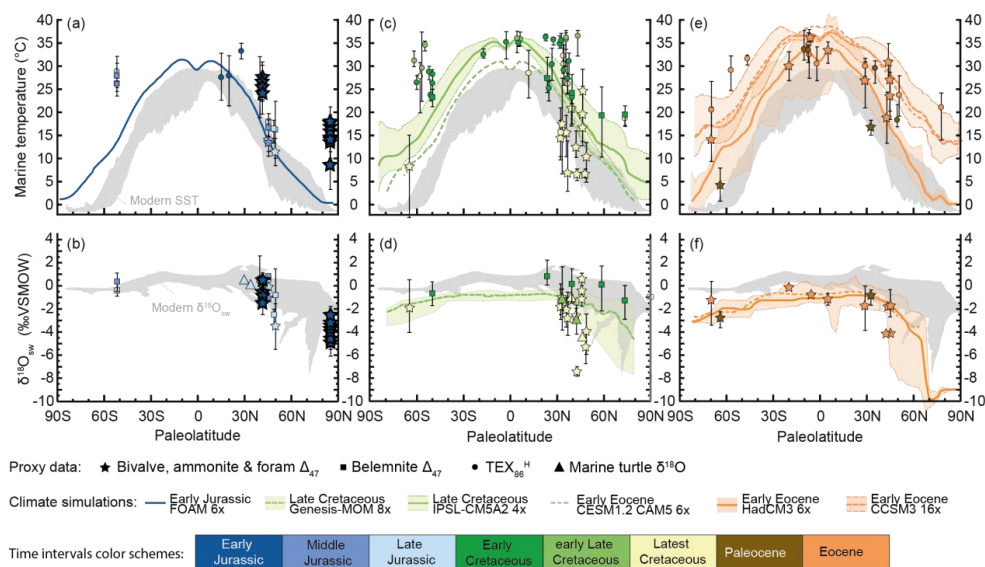
Figure 5. Comparison of the new (bold outline) reconstructed Early Jurassic SST and δ^{18}O$_{sw}$ with Jurassic-Eocene proxy-based reconstructions (thin outline) and Earth system simulations. Proxy-model comparison of SST and δ18Osw are shown for the Jurassic (a, b), the Cretaceous (c, d) and the Early Paleogene (e, f). Marker colour in proxy data shows sample age (see key). Results of Earth system simulations are shown as annual averages (bold lines) and summer and winter seasonal averages (colour shading). See supplement for references used in this compilation.

6 Conclusion

The clumped isotope compositions of pristine, minimally buried, marine molluscs shells yield SST >25°C at mid-latitudes during the early Pliensbachian and SST >10°C at polar paleolatitudes during the T-OAE. The reconstructed δ^{18}O$_w$ values point to higher freshwater contribution toward Arctic regions, illustrating the dangers of assuming a fixed global δ^{18}O$_w$ value for δ^{18}O-derived temperature reconstructions. Although further work should clarify the influence of seasonal changes in the recorded SST values at polar sites, these results strengthen a growing body of evidence for higher climate sensitivity under high atmospheric CO$_2$ conditions and suggest that this higher sensitivity is a general feature of greenhouse climates since at least 180 Ma.

Data availability

Detailed data supporting this study are available in the supplementary material. Raw data are available on request to the author.

Author contribution

TL and GS designed the study and led the writing in close cooperation with CL, MR and MD. MR and GS participated to the field work and collected the samples. TL prepared and sampled the shell material for geochemistry and performed the SEM observations. MR, JS and OL identified the fossils. MD and TL performed the clumped isotope analyses and data processing. AV-L and TL performed the stable isotopes

analyses and data processing. BR, GM and TL gathered and interpreted the Raman spectra. TL and GS compiled the paleotemperature proxy database. All authors were involved in the interpretation of the results.

355

Competing interest

The authors declare that they have no conflict of interest.

Acknowledgments

360   This research was funded by the ANR OXYMORE (ANR-18-CE31-0020) and RFBR grant 21-55-15015. We thank Ghislaine Broillet for her help with SEM analyses, and Ophélie Lodyga for help with Raman analyses.

References

365 Anderson, N. T., Kelson, J. R., Kele, S., Daëron, M., Bonifacie, M., Horita, J., Mackey, T. J., John, C. M., Kluge, T., Petschnig, P., Jost, A. B., Huntington, K. W., Bernasconi, S. M., and Bergmann, K. D.: A unified clumped isotope thermometer calibration (0.5–1100°C) using carbonate-based standardization, Geophys Res Lett, https://doi.org/10.1029/2020GL092069, 2021.

Baghli, H., Mattioli, E., Spangenberg, J. E., Bensalah, M., Arnaud-Godet, F., Pittet, B., and Suan, G.:
370 Early Jurassic climatic trends in the south-Tethyan margin, 15, 2020.

Bernasconi, S. M., Müller, I. A., Bergmann, K. D., Breitenbach, S. F. M., Fernandez, A., Hodell, D. A., Jaggi, M., Meckler, A. N., Millan, I., and Ziegler, M.: Reducing Uncertainties in Carbonate Clumped Isotope Analysis Through Consistent Carbonate-Based Standardization, Geochem. Geophys. Geosyst., 19, 2895–2914, https://doi.org/10.1029/2017GC007385, 2018.

375 Bernasconi, S. M., Daëron, M., Bergmann, K. D., Bonifacie, M., Meckler, A. N., Affek, H. P., Anderson, N., Bajnai, D., Barkan, E., Beverly, E., Blamart, D., Burgener, L., Calmels, D., Chaduteau, C., Clog, M., Davidheiser-Kroll, B., Davies, A., Dux, F., Eiler, J., Elliott, B., Fetrow, A. C., Fiebig, J., Goldberg, S., Hermoso, M., Huntington, K. W., Hyland, E., Ingalls, M., Jaggi, M., John, C. M., Jost, A. B., Katz, S., Kelson, J., Kluge, T., Kocken, I. J., Laskar, A., Leutert, T. J., Liang, D., Lucarelli, J.,
380 Mackey, T. J., Mangenot, X., Meinicke, N., Modestou, S. E., Müller, I. A., Murray, S., Neary, A., Packard, N., Passey, B. H., Pelletier, E., Petersen, S., Piasecki, A., Schauer, A., Snell, K. E., Swart, P. K., Tripati, A., Upadhyay, D., Vennemann, T., Winkelstern, I., Yarian, D., Yoshida, N., Zhang, N., and Ziegler, M.: InterCarb: A Community Effort to Improve Interlaboratory Standardization of the Carbonate Clumped Isotope Thermometer Using Carbonate Standards, Geochem Geophys Geosyst,
385 22, https://doi.org/10.1029/2020GC009588, 2021.

Blaise, T., Barbarand, J., Kars, M., Ploquin, F., Aubourg, C., Brigaud, B., Cathelineau, M., El Albani, A., Gautheron, C., Izart, A., Janots, D., Michels, R., Pagel, M., Pozzi, J.-P., Boiron, M.-C., and Landrein, P.: Reconstruction of low temperature (<100 °C) burial in sedimentary basins: A comparison of geothermometer in the intracontinental Paris Basin, Marine and Petroleum Geology,
390 53, 71–87, https://doi.org/10.1016/j.marpetgeo.2013.08.019, 2014.

Buick, D. P. and Ivany, L. C.: 100 years in the dark: Extreme longevity of Eocene bivalves from Antarctica, Geology, 32, 921–924, https://doi.org/10.1130/G20796.1, 2004.

Coulson, A. B., Kohn, M. J., and Barrick, R. E.: Isotopic evaluation of ocean circulation in the Late Cretaceous North American seaway, Nature Geosci, 4, 852–855, https://doi.org/10.1038/ngeo1312,
395 2011.

Craig, N.: Growth of the bivalve Nucula annulata in nutrient-enriched environments, Mar. Ecol. Prog. Ser., 104, 77–90, https://doi.org/10.3354/meps104077, 1994.

Daëron, M.: Full Propagation of Analytical Uncertainties in Δ_{47} Measurements, Geochem Geophys Geosyst, 22, https://doi.org/10.1029/2020GC009592, 2021.

400 Daëron, M., Blamart, D., Peral, M., and Affek, H. P.: Absolute isotopic abundance ratios and the accuracy of $\Delta 47$ measurements, Chemical Geology, 442, 83–96, https://doi.org/10.1016/j.chemgeo.2016.08.014, 2016.

Dera, G. and Donnadieu, Y.: Modeling evidences for global warming, Arctic seawater freshening, and sluggish oceanic circulation during the Early Toarcian anoxic event, Paleoceanography, 27, n/a-n/a,
405 https://doi.org/10.1029/2012PA002283, 2012.

Dera, G., Pucéat, E., Pellenard, P., Neige, P., Delsate, D., Joachimski, M. M., Reisberg, L., and Martinez, M.: Water mass exchange and variations in seawater temperature in the NW Tethys during the Early Jurassic: Evidence from neodymium and oxygen isotopes of fish teeth and belemnites, Earth and Planetary Science Letters, 286, 198–207, https://doi.org/10.1016/j.epsl.2009.06.027, 2009.

410 van Dijk, J., Fernandez, A., Bernasconi, S. M., Caves Rugenstein, J. K., Passey, S. R., and White, T.: Spatial pattern of super-greenhouse warmth controlled by elevated specific humidity, Nature Geoscience, 13, 739–744, https://doi.org/10.1038/s41561-020-00648-2, 2020.

Disnar, J. R., Le Strat, P., Farjanel, G., and Fikri, A.: Sédimentation de la matière organique dans le nord-est du Bassin de Paris: conséquences sur le dépôt des argilites carbonées du Toarcien inférieur
415 (Organic matter sedimentation in the northeast of the Paris Basin: consequences on the deposition of the lower toarcian black shales), Chemical Geology, 131, 15–35, https://doi.org/10.1016/0009-2541(96)00021-6, 1996.

Douglas, P. M. J., Affek, H. P., Ivany, L. C., Houben, A. J. P., Sijp, W. P., Sluijs, A., Schouten, S., and Pagani, M.: Pronounced zonal heterogeneity in Eocene southern high-latitude sea surface
420 temperatures, Proceedings of the National Academy of Sciences, 111, 6582–6587, https://doi.org/10.1073/pnas.1321441111, 2014.

Epstein, S., Buchsbaum, R., Lowenstam, H. A., and Urey, H. C.: Revised carbonate-water isotopic temperature scale, Geol Soc America Bull, 64, 1315, https://doi.org/10.1130/0016-7606(1953)64[1315:RCITS]2.0.CO;2, 1953.

425 Evans, D., Sagoo, N., Renema, W., Cotton, L. J., Müller, W., Todd, J. A., Saraswati, P. K., Stassen, P., Ziegler, M., Pearson, P. N., Valdes, P. J., and Affek, H. P.: Eocene greenhouse climate revealed by coupled clumped isotope-Mg/Ca thermometry, Proc Natl Acad Sci USA, 115, 1174–1179, https://doi.org/10.1073/pnas.1714744115, 2018.

Fernandez, A., Korte, C., Ullmann, C. V., Looser, N., Wohlwend, S., and Bernasconi, S. M.:
430 Reconstructing the magnitude of Early Toarcian (Jurassic) warming using the reordered clumped isotope compositions of belemnites, 293, 308–327, https://doi.org/10.1016/j.gca.2020.10.005, 2021.

Grossman, E. L. and Ku, T.-L.: Oxygen and carbon isotope fractionation in biogenic aragonite: temperature effects, 59, 59–74, https://doi.org/10.1016/0168-9622(86)90057-6, 1986.

Hemingway, J. D. and Henkes, G. A.: A disordered kinetic model for clumped isotope bond
435 reordering in carbonates, Earth and Planetary Science Letters, 566, 116962, https://doi.org/10.1016/j.epsl.2021.116962, 2021.

Henkes, G. A., Passey, B. H., Grossman, E. L., Shenton, B. J., Pérez-Huerta, A., and Yancey, T. E.:
Temperature limits for preservation of primary calcite clumped isotope paleotemperatures,
Geochimica et Cosmochimica Acta, 139, 362–382, https://doi.org/10.1016/j.gca.2014.04.040, 2014.

440   van Hinsbergen, D. J. J., de Groot, L. V., van Schaik, S. J., Spakman, W., Bijl, P. K., Sluijs, A.,
Langereis, C. G., and Brinkhuis, H.: A Paleolatitude Calculator for Paleoclimate Studies, PLOS ONE,
10, e0126946, https://doi.org/10.1371/journal.pone.0126946, 2015.

Huber, M. and Caballero, R.: The early Eocene equable climate problem revisited, 7, 603–633,
https://doi.org/10.5194/cp-7-603-2011, 2011.

445   Jenkyns, H. C. and Clayton, C. J.: Black shales and carbon isotopes in pelagic sediments from the
Tethyan Lower Jurassic, Sedimentology, 33, 87–106, https://doi.org/10.1111/j.1365-
3091.1986.tb00746.x, 1986.

Jenkyns, H. C., Forster, A., Schouten, S., and Sinninghe Damsté, J. S.: High temperatures in the Late
Cretaceous Arctic Ocean, Nature, 432, 888–892, https://doi.org/10.1038/nature03143, 2004.

450   Kerimov, V. Yu., Shcherbina, Yu. V., and Ivanov, A. A.: Formation conditions and evolution of oil
and gas source strata of the Laptev sea shelf ore and gas province, Izvestiya Vysshikh Uchebnykh
Zavedeniy. Geologiya i Razvedka, 46–59, https://doi.org/10.32454/0016-7762-2020-63-3-46-59,
2020.

Killam, D. E. and Clapham, M. E.: Identifying the ticks of bivalve shellL clocks: seasonal growth in
455   relation to temperature and food supply, 33, 228–236, https://doi.org/10.2110/palo.2017.072, 2018.

Kim, S.-T. and O'Neil, J. R.: Equilibrium and nonequilibrium oxygen isotope effects in synthetic
carbonates, Geochimica et Cosmochimica Acta, 61, 3461–3475, https://doi.org/10.1016/S0016-
7037(97)00169-5, 1997.

Kim, S.-T., Mucci, A., and Taylor, B. E.: Phosphoric acid fractionation factors for calcite and
460   aragonite between 25 and 75 °C: Revisited, Chemical Geology, 246, 135–146,
https://doi.org/10.1016/j.chemgeo.2007.08.005, 2007.

Krencker, F. N., Bodin, S., Hoffmann, R., Suan, G., Mattioli, E., Kabiri, L., Föllmi, K. B., and
Immenhauser, A.: The middle Toarcian cold snap: Trigger of mass extinction and carbonate factory
demise, 15, 2014.

465   Laugié, M., Donnadieu, Y., Ladant, J.-B., Green, J. A. M., Bopp, L., and Raisson, F.: Stripping back
the modern to reveal the Cenomanian–Turonian climate and temperature gradient underneath, Clim.
Past, 16, 953–971, https://doi.org/10.5194/cp-16-953-2020, 2020.

Li, X., Wang, J., Rasbury, T., Zhou, M., Wei, Z., and Zhang, C.: Early Jurassic climate and
atmospheric CO_2 concentration in the Sichuan paleobasin, southwestern China, 16, 2055–2074,
470   https://doi.org/10.5194/cp-16-2055-2020, 2020.

McElwain, J. C., Wade-Murphy, J., and Hesselbo, S. P.: Changes in carbon dioxide during an oceanic
anoxic event linked to intrusion into Gondwana coals, Nature, 435, 479–482,
https://doi.org/10.1038/nature03618, 2005.

Nikitenko, B. L. and Mickey, M. B.: Foraminifera and ostracodes across the Pliensbachian-Toarcian
475   boundary in the Arctice Realm (stratigraphy, palaeobiogeography and biofacies), 230, 137–174,
https://doi.org/10.1144/GSL.SP.2004.230.01.08, 2004.

Nikitenko, B. L., Shurygin, B. N., Knyazev, V. G., Meledina, S. V., Dzyuba, O. S., Lebedeva, N. K.,
Peshchevitskaya, E. B., Glinskikh, L. A., Goryacheva, A. A., and Khafaeva, S. N.: Jurassic and

480   Cretaceous stratigraphy of the Anabar area (Arctic Siberia, Laptev Sea coast) and the Boreal zonal
        standard, Russian Geology and Geophysics, 54, 808–837, https://doi.org/10.1016/j.rgg.2013.07.005,
        2013.

        Nooitgedacht, C. W., van der Lubbe, H. J. L., Ziegler, M., and Staudigel, P. T.: Internal water
        facilitates thermal resetting of clumped isotopes in biogenic aragonite, Geochem Geophys Geosyst,
        https://doi.org/10.1029/2021GC009730, 2021.

485   O'Brien, C. L., Robinson, S. A., Pancost, R. D., Sinninghe Damsté, J. S., Schouten, S., Lunt, D. J.,
        Alsenz, H., Bornemann, A., Bottini, C., Brassell, S. C., Farnsworth, A., Forster, A., Huber, B. T.,
        Inglis, G. N., Jenkyns, H. C., Linnert, C., Littler, K., Markwick, P., McAnena, A., Mutterlose, J.,
        Naafs, B. D. A., Püttmann, W., Sluijs, A., van Helmond, N. A. G. M., Vellekoop, J., Wagner, T., and
        Wrobel, N. E.: Cretaceous sea-surface temperature evolution: Constraints from TEX 86 and
490   planktonic foraminiferal oxygen isotopes, Earth-Science Reviews, 172, 224–247,
        https://doi.org/10.1016/j.earscirev.2017.07.012, 2017.

        Pagani, M., Pedentchouk, N., Huber, M., Sluijs, A., Schouten, S., Brinkhuis, H., Damste, J. S. S., and
        Dickens, G. R.: Arctic hydrology during global warming at the Palaeocene/Eocene thermal maximum,
        442, 671–675, https://doi.org/10.1038/nature05043, 2006.

495   Peck, L. S., Colman, J. G., and Murray, A. W. A.: Growth and tissue mass cycles in the infaunal
        bivalve Yoldia eightsi at Signy Island, Antarctica, Polar Biology, 23, 420–428,
        https://doi.org/10.1007/s003000050463, 2000.

        Petersen, S. V., Tabor, C. R., Lohmann, K. C., Poulsen, C. J., Meyer, K. W., Carpenter, S. J.,
        Erickson, J. M., Matsunaga, K. K. S., Smith, S. Y., and Sheldon, N. D.: Temperature and salinity of
500   the Late Cretaceous Western Interior Seaway, Geology, 44, 903–906,
        https://doi.org/10.1130/G38311.1, 2016.

        Pucéat, E., Lécuyer, C., Sheppard, S. M. F., Dromart, G., Reboulet, S., and Grandjean, P.: Thermal
        evolution of Cretaceous Tethyan marine waters inferred from oxygen isotope composition of fish
        tooth enamels, Paleoceanography, 18, n/a-n/a, https://doi.org/10.1029/2002PA000823, 2003.

505   Robinson, S. A., Ruhl, M., Astley, D. L., Naafs, B. D. A., Farnsworth, A. J., Bown, P. R., Jenkyns, H.
        C., Lunt, D. J., O'Brien, C., Pancost, R. D., and Markwick, P. J.: Early Jurassic North Atlantic sea-
        surface temperatures from TEX 86 palaeothermometry, Sedimentology, 64, 215–230,
        https://doi.org/10.1111/sed.12321, 2017.

        Roche, D. M., Donnadieu, Y., Pucéat, E., and Paillard, D.: Effect of changes in δ^{18}O content of the
510   surface ocean on estimated sea surface temperatures in past warm climate, Paleoceanography, 21, n/a-
        n/a, https://doi.org/10.1029/2005PA001220, 2006.

        Rogov, M. A., Zverkov, N. G., Zakharov, V. A., and Arkhangelsky, M. S.: Marine Reptiles and
        Climates of the Jurassic and Cretaceous of Siberia, Stratigr. Geol. Correl., 27, 398–423,
        https://doi.org/10.1134/S0869593819040051, 2019.

515   Rozanski, K., Araguas-Araguas, L., and Gonfiantini, R.: Relation Between Long-Term Trends of
        Oxygen-18 Isotope Composition of Precipitation and Climate, Science, 258, 981–985,
        https://doi.org/10.1126/science.258.5084.981, 1992.

        Ruebsam, W., Reolid, M., Sabatino, N., Masetti, D., and Schwark, L.: Molecular paleothermometry of
        the early Toarcian climate perturbation, 195, 103351, https://doi.org/10.1016/j.gloplacha.2020.103351,
520   2020.

Schöne, B. R.: The curse of physiology—challenges and opportunities in the interpretation of geochemical data from mollusk shells, Geo-Mar Lett, 28, 269–285, https://doi.org/10.1007/s00367-008-0114-6, 2008.

525 Shackleton, N. J. and Kennett, J. P.: Paleotemperature history of the Cenozoic and the initiation of Antarctic glaciation: oxygen and carbon isotope analyses in DSDP Sites 277,279, and 281, 29, 743–756, 1975.

Sluijs, A., Schouten, S., Pagani, M., Woltering, M., Brinkhuis, H., Damsté, J. S. S., Dickens, G. R., Huber, M., Reichart, G.-J., Stein, R., Matthiessen, J., Lourens, L. J., Pedentchouk, N., Backman, J., Moran, K., and the Expedition 302 Scientists: Subtropical Arctic Ocean temperatures during the
530 Palaeocene/Eocene thermal maximum, Nature, 441, 610–613, https://doi.org/10.1038/nature04668, 2006.

Sluijs, A., Frieling, J., Inglis, G. N., Nierop, K. G. J., Peterse, F., Sangiorgi, F., and Schouten, S.: Late Paleocene – early Eocene Arctic Ocean Sea Surface Temperatures; reassessing biomarker paleothermometry at Lomonosov Ridge, Proxy Use-Development-Validation/Marine
535 Archives/Cenozoic, https://doi.org/10.5194/cp-2020-13, 2020.

Stolper, D. A. and Eiler, J. M.: The kinetics of solid-state isotope-exchange reactions for clumped isotopes: A study of inorganic calcites and apatites from natural and experimental samples, 315, 363–411, https://doi.org/10.2475/05.2015.01, 2015.

Suan, G., Mattioli, E., Pittet, B., Lécuyer, C., Suchéras-Marx, B., Duarte, L. V., Philippe, M.,
540 Reggiani, L., and Martineau, F.: Secular environmental precursors to Early Toarcian (Jurassic) extreme climate changes, 11, 2010.

Suan, G., Nikitenko, B. L., Rogov, M. A., Baudin, F., Spangenberg, J. E., Knyazev, V. G., Glinskikh, L. A., Goryacheva, A. A., Adatte, T., Riding, J. B., Föllmi, K. B., Pittet, B., Mattioli, E., and Lécuyer, C.: Polar record of Early Jurassic massive carbon injection, Earth and Planetary Science Letters, 312,
545 102–113, https://doi.org/10.1016/j.epsl.2011.09.050, 2011.

Suan, G., Popescu, S.-M., Suc, J.-P., Schnyder, J., Fauquette, S., Baudin, F., Yoon, D., Piepjohn, K., Sobolev, N. N., and Labrousse, L.: Subtropical climate conditions and mangrove growth in Arctic Siberia during the early Eocene, 45, 539–542, https://doi.org/10.1130/G38547.1, 2017.

Thierry, J.: Middle Toarcian map. 8, in: Dercourt, J., Gaetani, M., Vrielynck, B., Barrier, E., Biju-
550 Duval, B., Brunet, M.F. ... Sandulescu, M. (Eds.), Altlas Peri-Tethys Palaeogeographical Maps., CCGM/CGMW, Paris, 61–70, 2000.

Thuy, B., Gale, A. S., and Reich, M.: A new echinoderm Lagerstätte from the Pliensbachian (Early Jurassic) of the French Ardennes, Swiss J Palaeontol, 130, 173–185, https://doi.org/10.1007/s13358-010-0015-y, 2011.

555 Tindall, J., Flecker, R., Valdes, P., Schmidt, D. N., Markwick, P., and Harris, J.: Modelling the oxygen isotope distribution of ancient seawater using a coupled ocean–atmosphere GCM: Implications for reconstructing early Eocene climate, Earth and Planetary Science Letters, 292, 265–273, https://doi.org/10.1016/j.epsl.2009.12.049, 2010.

Torsvik, T. H., Van der Voo, R., Preeden, U., Mac Niocaill, C., Steinberger, B., Doubrovine, P. V.,
560 van Hinsbergen, D. J. J., Domeier, M., Gaina, C., Tohver, E., Meert, J. G., McCausland, P. J. A., and Cocks, L. R. M.: Phanerozoic polar wander, palaeogeography and dynamics, Earth-Science Reviews, 114, 325–368, https://doi.org/10.1016/j.earscirev.2012.06.007, 2012.

Ullmann, C. V., Boyle, R., Duarte, L. V., Hesselbo, S. P., Kasemann, S. A., Klein, T., Lenton, T. M., Piazza, V., and Aberhan, M.: Warm afterglow from the Toarcian Oceanic Anoxic Event drives the success of deep-adapted brachiopods, Sci Rep, 10, 6549, https://doi.org/10.1038/s41598-020-63487-6, 2020.

565

Vihtakari, M., Renaud, P. E., Clarke, L. J., Whitehouse, M. J., Hop, H., Carroll, M. L., and Ambrose, W. G.: Decoding the oxygen isotope signal for seasonal growth patterns in Arctic bivalves, Palaeogeography, Palaeoclimatology, Palaeoecology, 446, 263–283, https://doi.org/10.1016/j.palaeo.2016.01.008, 2016.

570

Waterlot, G., Bonte, A., and Destombes, J.-P.: Carte géologique de la France à 1:50 000. [68], Renwez, France, 1960.

Zakharov, V. A. and Shurygin, B. N.: Biogeography, facies and stratigraphy of the Middle Jurassic of Soviet Arctic (by bivalve molluscs), 352, 1–206, 1978.

575   Zhou, J., Poulsen, C. J., Pollard, D., and White, T. S.: Simulation of modern and middle Cretaceous marine δ^{18}O with an ocean-atmosphere general circulation model: Modern, mid-Cretaceous seawater δ^{18}O, Paleoceanography, 23, n/a-n/a, https://doi.org/10.1029/2008PA001596, 2008.

Zhu, J., Poulsen, C. J., Otto-Bliesner, B. L., Liu, Z., Brady, E. C., and Noone, D. C.: Simulation of early Eocene water isotopes using an Earth system model and its implication for past climate
580   reconstruction, Earth and Planetary Science Letters, 537, 116164, https://doi.org/10.1016/j.epsl.2020.116164, 2020.